Ceramics International 47 (2021) 15931–15938

Contents lists available at ScienceDirect

Ceramics International

journal homepage: www.elsevier.com/locate/ceramint

Study of mixing process of low temperature co-fired ceramics photocurable suspension for digital light processing stereolithography

J.G. Fernandes [a,b,c], P. Barcelona [c], M. Blanes [a,b], J.A. Padilla [c], F. Ramos [a], A. Cirera [b], E. Xuriguera [c,*]

[a] FAE, Francisco Albero S.A.U, C/Rafael Barradas, 19, Polig. Gran Via Sud, 08908 L'Hospitalet de Llobregat, Barcelona, Spain
[b] Universitat de Barcelona, Department of Electronic and Biomedical Engineering, C/ Martí I Franquès, 1, 08028, Barcelona, Spain
[c] Universitat de Barcelona, Department of Materials Science and Physical Chemistry, C/ Martí I Franquès, 1, 08028, Barcelona, Spain

ARTICLE INFO

Keywords:
Additive manufacturing
Low temperature Co-Fired ceramics
Digital light processing stereolithography
Slurry mixing method

ABSTRACT

The Low Temperature Co-fired Ceramic (LTCC) materials are highly used for high frequency devices required for high-speed data communications, representing an attractive material for electronic applications with a direct industrial applicability. The development of a photocurable LTCC suspension for Digital Light Processing Stereolithography (DLP-SLA) technology is presented in this work. The LTCC suspension, with an optimal solid load of 40.4 vol%, was characterized along its preparation regarding the rheological behaviour, dispersant content, particle size distribution in function of milling time and photocuring properties in a visible light range. The effect of the particle size change, through ball milling, on viscosity and photocuring behaviour was studied, achieving an optimal mixing range time, which highlights the importance of the manufacturing standardization of the photocurable suspensions. The optimized suspension presents a viscosity of 3.6 Pa s at shear rate of 2 s^{-1}, a sensitivity of 41 μm and a critical energy dose of 15 mJ cm^{-2}. The printing process was successfully achieved, demonstrated by some defect-free printed pieces.

1. Introduction

From a technological point of view, Additive Manufacturing (AM) offers an entirely new palette of geometries to play with in the manufacturing of new objects. Thanks to AM, the current concept of product development has been reshaped, opening the door to a new level of customization. A very much valued characteristic of AM in this fast-paced world is that it allows companies to quickly respond to industry and customer feedback, taking advantage of the latest technologies. Nowadays, ceramic materials have claimed their role in AM, mainly for high temperature [1–4] and biomedical applications [5–9]. However, it is well known that ceramic materials generally possess low toughness, low ductility, and high crack damage sensitivity, which combined with the high hardness and high melting temperatures, make them difficult to handle during manufacturing. Furthermore, ceramic materials are also applied to electronic applications [10,11] where multi-material systems are often needed in order to develop functional components, which add further challenges to the manufacturing process. Currently, the design and manufacture of electronic components based on Low Temperature Co-fired Ceramic (LTCC) materials process requires different technologies such as tape casting, screen printing, filling vias, stacking, cutting, and lamination, apart from the ceramic suspension preparation and the de-binding and sintering of the green body [12,13]. Moreover, in the screen-printing step each re-design needs a new screen pattern, increasing the development costs and time-to-market. Thus, one possibility to improve this technological drawback can be AM of multi-material. For this to happen, the hybridization of AM technologies is a key strategy enhancing the individual technologies' capabilities [14–18]. The LTCC materials are glass-ceramic composites, where the main phase is a dielectric such as alumina which have a high sintering temperature (1650 °C). However, the addition of a glass phase to the dielectric material lowers the sintering temperature, below 950 °C, depending on the amount and type of the glass composition [19]. In this regard, the low sintering temperature provided by the LTCC materials is one of the key issues of these materials when compared with the High Temperature Co-fired Ceramics (HTCC). The sintering process at low temperatures allows the fabrication of the embedded electronic components using common and highly conductive

* Corresponding author.
E-mail address: xuriguera@ub.edu (E. Xuriguera).

https://doi.org/10.1016/j.ceramint.2021.02.167
Received 20 January 2021; Received in revised form 12 February 2021; Accepted 18 February 2021
Available online 21 February 2021

metals such as silver or copper with low conductive loss and low electrical resistance at high frequencies. Apart from the low sintering temperature, LTCC materials have a lower dielectric loss at high frequencies when compared with polymeric materials or even with alumina, leading to a low loss of performance of the device [20].

The previous step of the printing process is the creation of a digital model, usually by a Computer-Aided Design (CAD) method. AM technologies requires the conversion of the CAD model into a STL file which uses triangles to describe the surface of the object, without any representation of colour, texture, or other common CAD model attributes. Once the STL file has been generated, the file is imported into a slicer program, slicing the 3D object into different layers considering the layer thickness of the printing process.

In the Digital Light Processing Stereolithography (DLP-SLA) technology, the fabrication of each layer is made by curing the whole layer in contrast with other additive manufacturing technologies (AMT), which are point by point. Thus, the slicer of the SLT file results in several 2D images, one for each layer. These images are composed of white and black pixels with a certain area, depending on the 3D model. In the white areas the light can pass through, resulting in the curing of these areas. On the other hand, the black areas block the light from passing through them, thus the photopolymerization of the resin is inhibited.

During the DLP-SLA process of ceramic materials, the photocurable resin is polymerized, trapping the ceramic particles on the crosslinked polymeric matrix, resulting in the green body which will further debinded and sintered. In our approach, the DLP-SLA machine uses a visible light projector as a light source and has a top-down configuration, enabling further integration for the printing of conductive materials on a ceramic substrate, such as inkjet system or robocasting. The recoating of each layer along the DLP-SLA printing process is achieved by a so-called deep dip system assisted by a wiper [20]. Regarding the de-binding and sintering processes, the LTCC suspension must contain a high ceramic concentration (>40 vol%) [21–24] to prevent defect formation (cracks and delamination) and to maximize the density of the sintered part [22,25]. On the other hand, as the recoating system of the developed machine is by dipping the part into the uncured resin, the viscosity should be the lowest possible and not higher than 5 Pa s at low shear rates, for a proper recoating [20,24]. Another important factor is the photocuring behaviour, which must consider a proper sensitivity of LTCC suspension in the range of visible light.

The LTCC material is highly used for electronic application, thus at least two different material are needed during the manufacturing of the devices. In on hand the LTCC as a substrate and, on the other the conductive material for the signal transmission/reception. In the presented work, the development and optimization of the LTCC photocurable suspension for DLP-SLA is presented as a first step for the further technology hybridization for the multimaterial printing (such as DLP-SLA and material jetting or material extrusion-based technologies).

2. Experimental procedure

2.1. Materials

A commercial acrylate-based resin with a phosphine oxide-type photoinitiator (SPOT-LV, Spot-A Materials) was used for the photocurable suspension, with a density of 1.1 g cm^{-3} and a viscosity of 42 mPa s (23 °C). The ceramic particles used is a LTCC powder based on a premixed lead-free blue barium borosilicate glass and alumina powder (51,528 B Glass Powder, HERAEUS) with a particle size, d_{50}, of 2.9 μm and a density of 3.38 g cm^{-3}. A biodegradable anionic dispersant based on the phosphate ester (Multitrope 1214, Croda) was used as a wetting agent and dispersant, to increase the homogeneity and reduce the agglomeration of the ceramic particles. Additionally, an antifoam (BYK 1794, BYK Additives & Instruments) was added to prevent air bubbles defects.

2.2. Preparation of photocurable suspensions

The homogenization of the LTCC suspension (LTCC powder, resin and dispersant) was achieved using horizontal ball milling. The preparation of the LTCC suspension was carried out in a polymeric jar with 3 mm alumina balls, adding all the compounds directly. The optimization of ceramic and dispersant content was carried out for 24 h with the previous detailed conditions with ceramic content of 3.6–50 vol% (10–75 wt%), and dispersant content of 0.25–2.00 wt% respect of the solid content.

The study about the dispersion process was carried out in the ball mill system for 305 h, to analyse the viscosity and photocuring behaviour evolution during the dispersion time, as the same time as particle size distribution of the particles in suspension. Samples were removed from the jar to perform all mentioned measurements at different mixing times.

After the milling process in the horizontal ball mill, a 0.4 wt% with respect to the total weight of antifoam was added into the final formulation following the manufacturer recommendations. This process was performed with a Thinky ARV-310 Planetary vacuum mixer at 2000 rpm at 36.9 kPa for 2 min, promoting the homogenization of the antifoam and aids the degassing of the suspension.

2.3. Rheological and photocuring characterization

The particle size of the raw powder and suspension particles was measured using MASTERSIZER 3000 from Malvern Panalytical, based on laser diffraction technology.

In addition, all rheological measurements were carried out on a Discovery HR-1 rheometer of TA Instruments with a 40 mm diameter plate-plate geometry and a gap of 0.5 mm at 23 °C controlled by a Peltier unit. All the measurements were performed by a logarithmic ascendant shear rate ramp, controlled by shear rate (CRS) mode, from 1 to 500 s^{-1}. To compare the viscosity curves of the suspensions with non-Newtonian behaviour, the viscosity value corresponding to shear rate of 2 s^{-1} has been chosen as reference.

The photocuring behaviour was defined by the working curve of each sample. The working curve plot is given by the relationship between the cure depth, C_d (μm), by means of the resultant cured thickness, caused by a certain applied energy dose, E_0 (mJ·cm^{-2}). This relationship is described by the Jacobs equation, equation (1) [26]:

$$C_d = D_p \ln\left(\frac{E_0}{E_c}\right) \quad \text{equation 1}$$

Where, D_p is the sensitivity in the depth direction, which has units of length and is related to an attenuation of the light through the printing direction. The relation between C_d and E_0 is commonly presented as a semi-logarithmic plot of C_d versus E_0 dose in logarithmic scale, where (1) the semi-logarithmic plot should result in a straight-line relationship, known as working curve, (2) the slope of the working curve is exactly the sensitivity, D_p, of the suspension and (3) the intercept of the working curve, i.e., the value of E_0 where $C_d = 0$ is precisely the critical energy dose, E_c(mJ·cm^{-2}). D_p and E_c, represents the two main characteristic of the suspension with certain composition and for a certain energy source. In the case of loaded resins with ceramic particles, the sensitivity of the resinD_p, is proportional to the average particle size (d_{50}) and inversely proportional to the ceramic volume fraction (Φ) and the materials scattering efficiency (S) [27,28].

To obtain these data, different energy doses must be applied by varying the exposure time to measure the resultant cured depth. The visible light projector used in the DLP-SLA machines is an Acer H6510BD, based on Digital Light Processing (DLP) technology, which has a maximum resolution of 1920 x 1200 pixels and a brightness of 3000 lm. Given the characteristics of the projector, it is possible to know the energy with which the sample is irradiated., where 683 lm corre-

sponds to a 1 W at ideal maximum luminous efficiency. Consequently, the effective power is around 4.39 W. However, the light projector is placed at 20 cm from the sample, projecting an area of 167 mm × 94 mm. In this regard, the projected energy is distributed throughout the projection area, thus it is convenient to know the irradiance which is 27.98 mW cm^{-2}. This value means that at each second the projector radiates an energy dose of 27.98 mJ cm^{-2}. This information is fundamental to graph the semi-logarithmic plot of C_d vs. E_0 for each sample. To standardize all measurements, a 2D square of 8.50 mm was projected and was collected data of the curing depth with a micrometre, tuning the exposure time.

2.4. Printing process and pieces characterization

A DLP-SLA printer, with a top-down configuration, was used to the 3D printing of specimens. In this approach, the visible light projector (Acer H6510BD) is placed on the top and the building platform goes down during the printing process. As already commented, this configuration gives the possibility to accoupling other AMT such as inkjet printing or robocasting, enabling the multi-material printing [29].

For this study, different batches of six pieces were printed with different layer thicknesses: 25, 50, and 75 μm, with the same exposure time of 10 s. A simple geometry was chosen to simplify its analysis. The selected geometry was a cylinder with a diameter of 10 mm, a height of 5 mm, and a wall thickness of 2 mm. After the printing process, all samples were cleaned with isopropanol and with air pressure to remove the uncured suspension.

As already shown by different authors the cure depth must be six times higher than the layer thickness to ensure a good bond between layers [30,31]. Thus, the propeller-like printed geometry was printed at 25 μm at layer thickness (z-direction) applying an energy dose of 520 mJ cm^{-2} meaning a 150 μm of cure depth.

The different samples were studied by Environmental Scanning Electron Microscopy Quanta 200 FEI (SEM) in surface and cross section.

For a deeper observation, the samples were studied by x-ray image analysis XT H 160 of Nikon to ensure a good layer adhesion, no delamination, and the absence of internal defects as air bubbles.

3. Results and discussions

3.1. Solid load and dispersant optimization

Regarding the de-binding and sintering processes, the LTCC suspension must contain a high ceramic concentration (>40 vol%) to prevent defect formation (cracks and delamination) and to maximize the density of the sintered part. On the other hand, the recoating system of the developed machine is by dipping the part into the uncured resin. This means that the viscosity should be the lowest possible and not higher than 5 Pa s at low shear rates (2 s^{-1}), for a proper recoating.

In this sense, the main objective of the following study is to maximize the ceramic load, taking into consideration the requirements imposed by the printing machine in terms of viscosity and photopolymerization behaviour. Different solid loads from 3.6 to 50 vol% (10–75 wt%) were studied at a constant dispersant content of 1 wt% respect the solid load.

In Fig. 1 is observed that the addition of ceramic powder drastically increases the viscosity, being more evident for volume fractions larger than 46 vol%. For example, the viscosity of the suspension with 40.4 vol % of LTCC presents a viscosity of 12 Pa s and by adding less than 6% of ceramic particles, the viscosity reaches values ten times higher (120 Pa s).

The suspensions with viscosity lower than 5 Pa s are the ones with a solid load lower than 33 vol% (doted lines in Fig. 1). Therefore, the two requirements are not achieved with this experiment. However, it is known that the optimization of both percentage of dispersant and milling time are two important parameters for the optimization of ceramic suspensions.

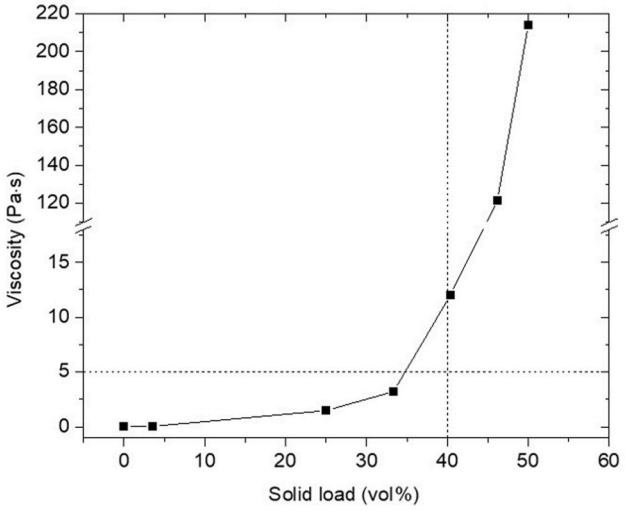

Fig. 1. Viscosity measured at a shear rate of 2 s^{-1} for different solid loads with 1 wt% of dispersant.

Therefore, the homogeneity and rheology of the ceramic suspension can be improved by adding the optimal amount of dispersant. In this study, a solid load of 40.4 vol% (67 wt%) and different dispersant content from 0.25 to 2.00 wt% were studied. The dispersant concentration was optimized for the lowest viscosity of the suspension, ensuring an optimal particle dispersion. Fig. 2 shows how the dispersant concentration affects the viscosity of the 67 wt% suspension.

For low dispersant concentrations, the particles are coated only partially with dispersant molecules, thus the stability and homogeneity of the system is not optimal. As the concentration of the dispersant increases, its molecules completely cover the particles, whereby the viscosity decreases, reaching a minimum which represents the highest stability level; as concentration increases, an increase of interactions between adsorbed chains of dispersant onto the particle surfaces increases the viscosity and the system is no longer in equilibrium.

Thus, it has been concluded that the optimum percentage of dispersant for this system corresponds to the minimum value of viscosity, that means at 1.5 wt% with respect to the solid contents. The optimization of the dispersants leads to a decrease of the viscosity, from 12 to 10 Pa s (dotted lines in Fig. 2), which still does not meet the target of having a viscosity lower than 5 Pa s. It is expected to achieve target

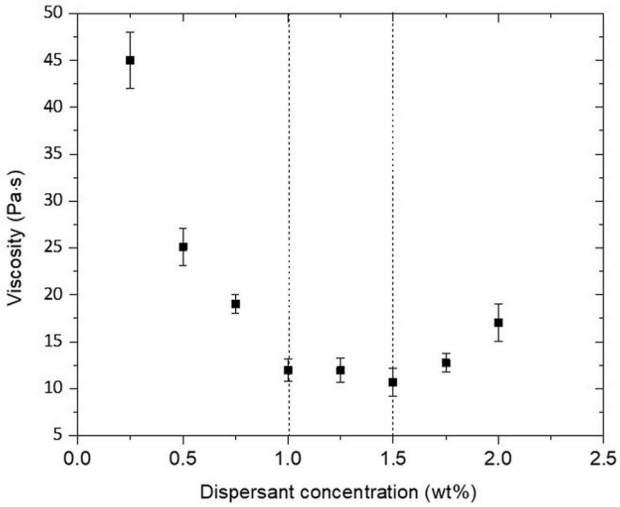

Fig. 2. Effect of the surfactant concentration on the viscosity (shear rate of 2 s^{-1}) for the 67 wt% LTCC suspension.

viscosity by optimizing the milling time, which is discussed in the following section.

3.2. Influence of the milling time on viscosity

The main objective of the milling process is to reduce the agglomerates and provide a better absorption of the dispersant onto the particle surface, improving the homogeneity of the LTCC suspension. Fig. 3 shows the viscosity values for each dispersing time at 2 s^{-1} of shear rate.

Three main zones can be clearly distinguished in this curve, regarding the viscosity tendency. Dotted lines were represented in Fig. 3 to emphasize these three zones with their corresponding numbers 1, 2, and 3. The principal characteristic of zone 1 is a decrease of the viscosity, which is more pronounced at the first 27 h, associated with the wetting of the powder. The effect of the movement of the balls becomes more effective increasing the adsorption of the dispersant onto the particles surface and the particles de-agglomeration, resulting in a reduction of attractive interactions between particles. Once the attractive forces between particles are reduced, the viscosity of the system drastically decreases. Another important factor that contributes to the drastic viscosity variation is that the balls mobility increases when the viscosity decreases, adding more energy to the system. Therefore, the homogenization of the suspension is accelerated. At the end of zone 1, between 27 and 52 h, the viscosity continues decreasing although at a lower rate.

Zone 2 is characterized as a constant zone, where the viscosity remains almost constant for a period of 40 h approximately. In this zone the minimum viscosity is achieved with a value of 2.8 Pa s. This means that in this zone the maximum dispersion of this system is achieved, i.e., the de-agglomeration of the particles is already accomplished and the dispersant absorption onto the particle surface reaches its maximum. In this regard, zone 2 is the period with the highest interest in terms of homogeneity and stability of the LTCC suspension, with a reduced amount of agglomerates and with the maximum absorption of the dispersant.

Zone 3 is delineated between 95 and 305 h of milling time, where the viscosity continuously increases with the milling time. The increase of the viscosity is explained with the reduction of the particle size due to the effective milling of the particles, which will be proven in the following section. Thus, if the milling process is in fact milling the ceramic particles, more particle surface area is being created. However, the amount of dispersant remains the same during the whole experiment which leads to a reduction of the ratio between the dispersant and particle surface area, resulting in an increase of the viscosity.

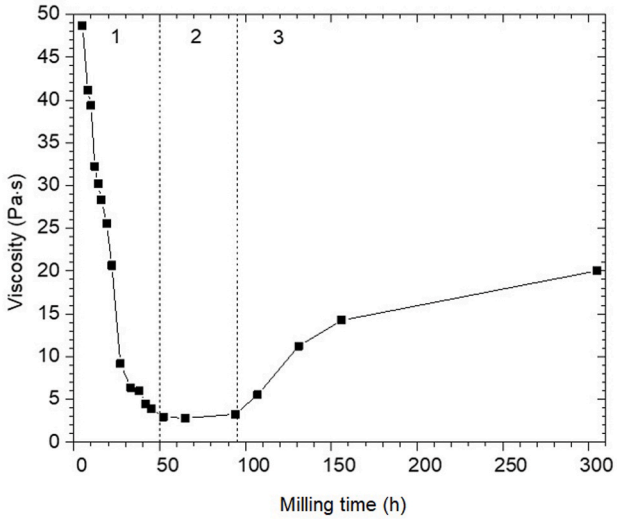

Fig. 3. Viscosity at shear rate of 2 s^{-1} vs milling time in ball mill.

3.3. Influence of particle size on viscosity

The particle size measurements were performed at each milling time for its correlation with the viscosity measurements and cure depth. Fig. 4 shows the particle size distribution in volume and cumulative. These results show the particle size distribution of the initial powder and for the suspension with 8, 65, and 305 h of milling time, exemplifying zone 1, zone 2, and zone 3, respectively. A bimodal distribution of all particle size distributions is observed in all cases.

The maximum values of particle size, d_{90}, decreases with the milling time, from 10 μm (powder) to 8 and 6 μm for the samples with 65 and 305 h of dispersing time, respectively. This means that the larger agglomerates/particles are being de-agglomerated/milled during this process. As a result, the particle size distribution is shifted to smaller values of particle size and becomes narrower as the milling time increases. Thus, two factors are being involved during the milling process: on one hand, the d_{50} decreases due to the de-agglomeration and/or milling of the agglomerates/particles and, on the other hand, the volume percentage at D_{50} increases once more superficial area is being formed with this de-agglomeration and/or milling. A deeper analysis of these overview results is shown below in Fig. 5, confirming the tendency presented in Fig. 4.

The particle size was measured at each milling time during the 305 h of the whole experiment. Fig. 5 shows the viscosity curve in function of the milling time with the particle size d_{50}.

It is observed that during the first 20 h (zone 1) the particle size remains almost constant. Hence, the viscosity reduction is mostly associated with adsorption of the dispersant onto the particle surface. Nevertheless, between 20 and 60 h, particles have a particle size reduction, increasing the specific surface area of the whole system. At the beginning of the milling process there is plenty of dispersant available in the system, thus the adsorption process onto the particles is faster when compared with the final stage of zone 1 (30–50 h). In this sense, the abrupt decrease of the viscosity between 5 and 30 h of milling time is related with the availability of the dispersant. In the final state of zone 1, the amount of free dispersant is not as much as at the beginning of the milling process, resulting in a slower absorption rate of the dispersant. At the same time, more specific surface area is being generated by the de-agglomeration, decreasing the relative proportion of dispersant amount to superficial area.

In zone 2 the viscosity remains almost constant, below the required value. However, in this zone the particle size decreases, consequently, more specific surface area is formed. Nonetheless, in this zone the

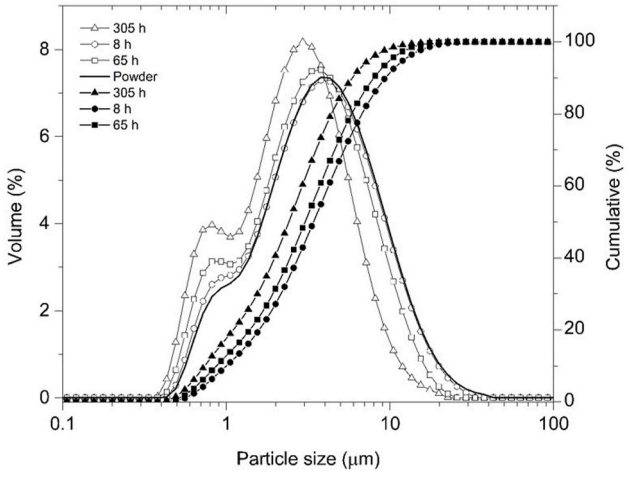

Fig. 4. Particle size distribution of the LTCC initial powder and of 8, 65, and 305 h of milling time of the LTCC suspension. Empty points correspond to particle size distribution in volume % and filled points correspond to cumulative %.

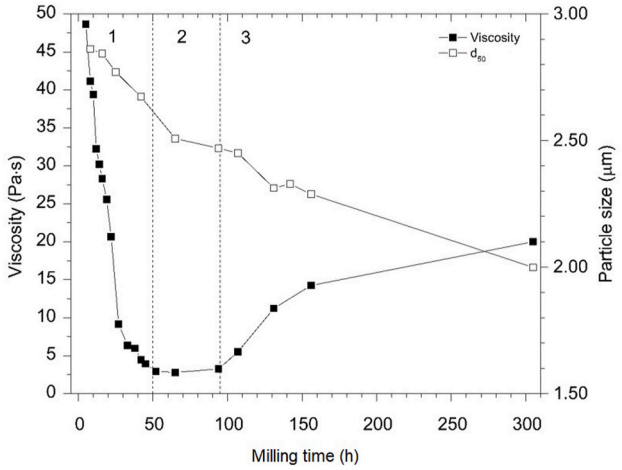

Fig. 5. Viscosity and particle size vs milling time.

viscosity value is the lowest of the whole study, which means that the mobility of the balls reaches its maximum, aiding the adsorption of the dispersant. Therefore, the viscosity remains constant for 40 h due to the balance between the generation of new specific surface area and absorption rate of the dispersant onto the particle surface, which increases by the higher mobility of the balls in this zone.

In zone 3 the viscosity increases, explained by the lack of dispersant available for the new surface formed by the de-agglomeration and/or milling of the particles, confirmed by the reduction of the particle size values. Thus, the increase of the superficial area and the lack of dispersant leads to an increase in the viscosity value.

3.4. Influence of particle size on photocuring behaviour

The photocuring behaviour was also studied during the milling process, analysing the cure depth along 305 h. In one hand, these results are directly associated with the sensitivity of the curing behaviour to the particle size changes and, on the other hand, will also serve to define the printing parameters. Fig. 6 shows the cure depth measured at an energy dose of 140 mJ cm^{-2}. The particle size for each milling time is also presented in this graphic to compare the effect of the particle size on the cure depth.

For the first 20 h of zone 1, the cure depth is almost constant which agrees with the particle size result, i.e., no changes of particle size results in a constant cure depth with an average value of 120 μm. After the first 20 h of the milling process, the cure depth decreases around 12.5% following the particle size reduction.

In zone 2 the variation of the cured depth becomes more gradual than in zone 1. In this zone the cure depth still decreases in value following the particle size reduction with the milling time, representing a 4.2% reduction in this zone. However, between 65 and 95 h, the cure depth is almost constant, around 100 μm, supported by the particle size values, which does not present a significant change.

In zone 3 the cure depth gradually decreases until 80 μm at 305 h. As the particle size decreases, the scattering of the light increases, which leads to the reduction of the cure depth.

Thus, as the solid load is constant in this experiment, the particle size reduction means an increase in the number of particles with a higher specific surface area. From a perspective of light scattering, more scattering points are being generated during the milling process, resulting in lower cure depth values. In other words, the increasing of the light scattering is an impediment for the light to penetrate through the ceramic suspension, limiting the polymerization of the resin. Therefore, the cure depth value decreases 33.3% at 305 h of dispersing time, with respect to the initial value of 120 μm.

To exemplify the difference in terms of E_c and the D_p at different dispersing times, one milling time was selected from the three different zones: 10 h for zone 1, 65 h for zone 2 and 305 h for zone 3. To calculate these values, the cure depth was measured at different energy doses to graph the working curve of each sample, represented in Fig. 7.

E_c is almost the same for all curves: close to 15 mJ cm^{-2}. However, D_p have different values: 49, 41, and 37 μm, for 10, 65, and 305 h of milling time, respectively. It is expected that the critical energy dose does not change, because this value is mainly affected by volume fraction of ceramic powder. However, a significant change of the slope is observed which results in a considerable variation of the sensitivity of the ceramic suspension; the lower the particle sizer, the higher the scattering phenomena and, consequently, the lower the sensitivity. Applying the same energy dose to the suspension, a lower cure depth is achieved for the samples with higher dispersion time.

Regarding both viscosity and photocuring behaviour, the range of milling time selected was between 65 and 95 h, within zone 2. At this range, the viscosity of the suspension reaches its minimum (2.8 Pa s at 2 s^{-1}) and, at the same time, the cure depth variation is almost constant (100 μm), representing the range where both factors remain almost constant. Once the LTCC suspension has almost the same characteristics in this milling time range, the optimum milling time was selected at 65 h, to ensure a good homogeneity and stability of the suspension.

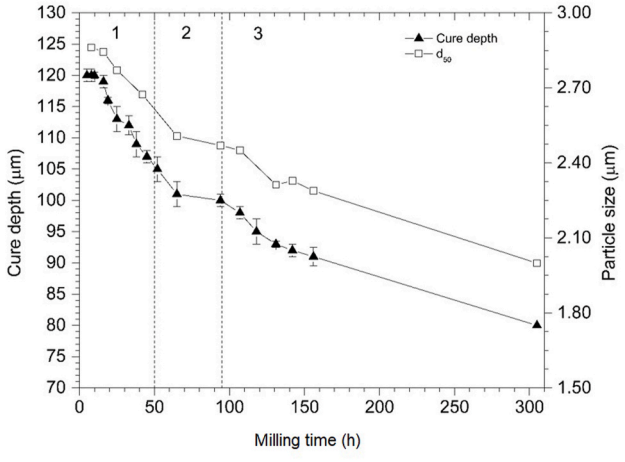

Fig. 6. Cure depth and particle size reduction vs milling time.

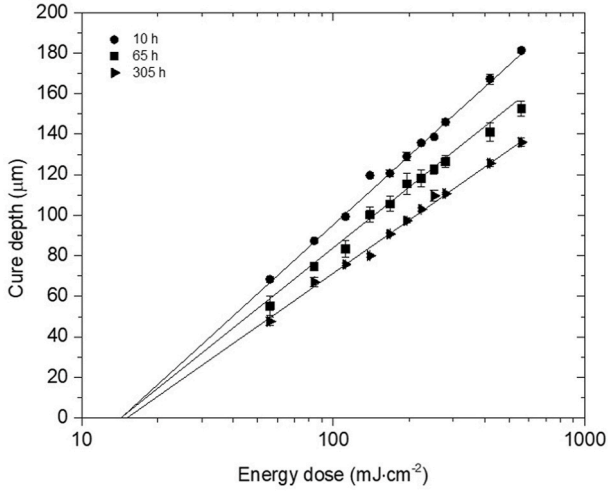

Fig. 7. Working curves for different milling time: 10, 65, and 305 h.

3.5. Influence of ceramic particle on rheological and photocuring behaviour

After the milling time, an antifoam was added to the LTCC suspension and rheological properties and photocurable behaviour were evaluated. Fig. 8 shows the viscosity plot of the SPOT LV, the optimized suspension and final suspension formulation with 67 wt% of LTCC powder.

An increase of two orders of magnitude of the viscosity is observed by adding the LTCC powder and, apart from that, the rheological behaviour changes from Newtonian to shear thinning behaviour, favourable to prevent/delay the sedimentation process. The addition of the antifoam leads to a slightly increase of the viscosity to values of 3.6 Pa s at 2 s^{-1}, however it is still lower than the maximum value required. Regarding the photocuring behaviour, no significant changes were observed by adding the antifoam.

Fig. 9 shows the comparison of the working curve of the SPOT LV resin and the final LTCC ceramic suspension. There is a clear change of the photocuring behaviour by adding the 67 wt% of ceramic powder, resulting in a $E_c = 48$ mJ cm^{-2} and $D_p = 850$ μm for the SPOT-LV and $E_c = 15$ mJ cm^{-2} and $D_p = 41$ μm for the LTCC suspension. The presence of ceramic particles reduces drastically the polymerization reaction, decreasing the sensitivity, by diluting the photoactive medium and attenuating light by scattering (reflection of the light by the particles).

3.6. Stability of the optimized suspension

The final LTCC suspension was studied in terms of its sedimentation for 5 months. The following results are related to the sedimentation test, which is performed to evaluate the stability of LTCC photocurable suspensions. In Fig. 10 is represented the results of the sedimentation test, showing a scheme used for the sedimentation evaluation. The LTCC suspension was dispensed into the measuring glass vials with a maximum height value of 3.5 cm and stored to rest in the dark. The sedimentation results are presented in term of resin percentage, i.e., resin height (h) with respect to the total height (H).

It was observed that for times shorter than 30 days, the separation of both phases, resin and LTCC suspension, are not sufficiently clear to be measured. Thus, the measurements are presented for times longer than 30 days. However, some initial phase separation evidence was visually detected after 10 days. The percentage of the resin fraction increases as the time increases, as a result of the sedimentation of the LTCC particles. Moreover, the maximum of the resin fraction tends to be 15%. The stability of the LTCC suspension is suitable for the printing process, once a phase separation is not detected during the first days. This means that the LTCC suspension could be used without sedimentation of the particles during the printing process.

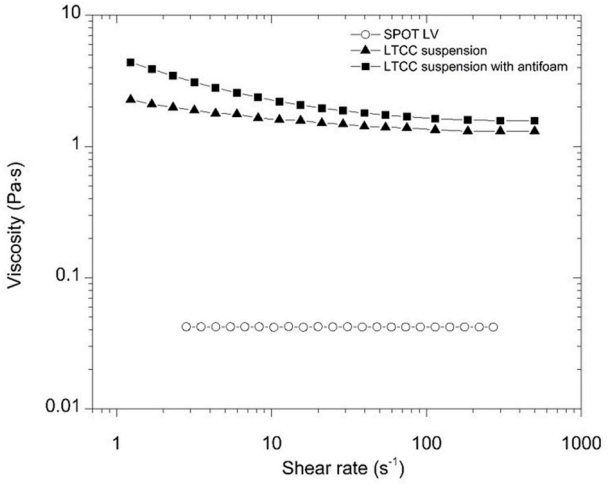

Fig. 8. Viscosity plot for the SPOT LV resin and for the optimized LTCC suspensions.

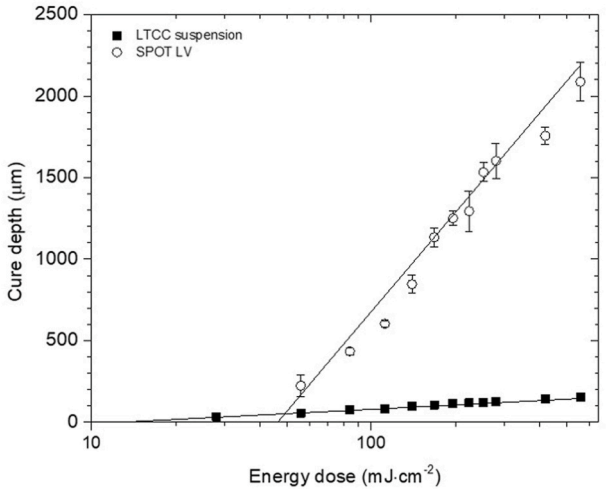

Fig. 9. Working curves of the SPOT LV resin and for the optimized LTCC suspension.

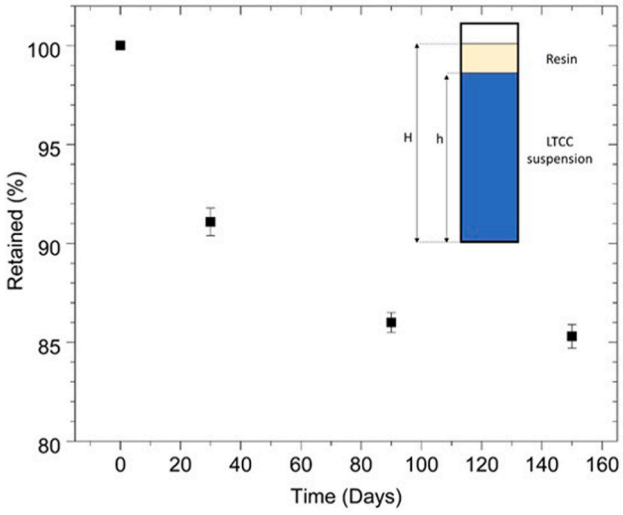

Fig. 10. Percentage of retained resin fraction vs resting time.

3.7. Printed pieces

The green bodies printed with optimized suspension (67 wt% of LTCC powder, 1.5 wt% of dispersant, 60 milling hours, 0.4 wt% antifoam) were studied using X-ray image and SEM. Fig. 11a, shows the X-ray images and Fig. 11b, SEM images of the cross-section (perpendicular to the XY-plane) of the printed cylinders at different layer thicknesses, 25, 50, and 75 μm, left to right respectively, at 10 s of exposure time (120 mJ cm^{-2}). X-ray images show the subject contrast to detect discontinuities present in pieces. Fig. 11a.1, Fig. 11a.2 and Fig. 11a.3, corresponding to pieces printed at 25, 50 and 75 μm of layer thickness respectively, present a minor printing defects in the central zone, marked on the figures. Tracking these defects during post-processing is a key point for determining how relevant they are to the process.

A wave-like effect at the surface is observed in the SEM images, Fig. 11b, due to the layer-by-layer building process. This effect is more evident for the pieces printed at 50 μm and 75 μm of layer thickness, highlighted in Fig. 11b.2 and Fig. 11b.3, respectively. The inner part of

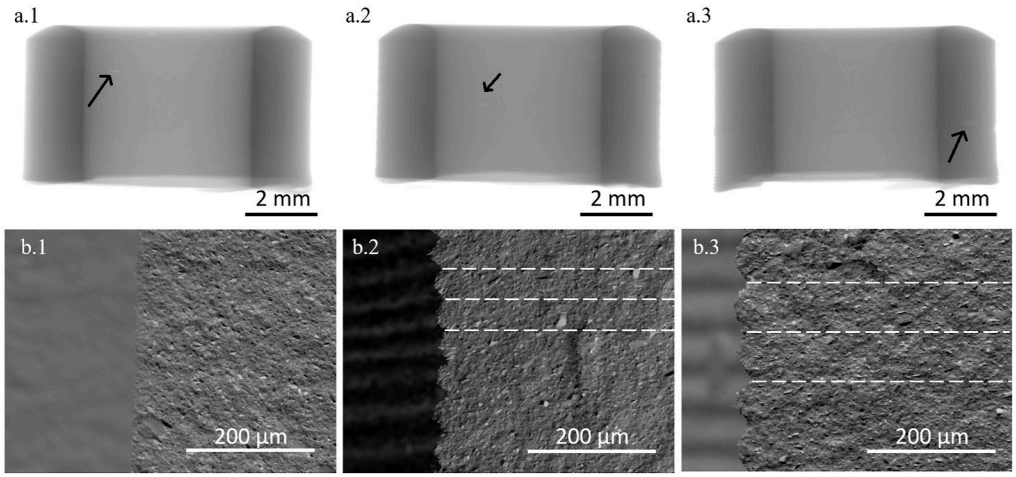

Fig. 11. X-ray images of the printed pieces at (a.1) 25 µm, (a.2) 50 µm and (a.3) 75 µm. SEM images of the printed pieces at (b.1) 25 µm, (b.2) 50 µm and (b.3) 75 µm.

all pieces is homogenous, where the layers cannot be identified nor evidence of delamination between layers is observed.

A de-binding and sintering process is required after printing to obtain the final ceramic piece, where the de-binding process is a critical step to achieve a ceramic piece without cracks. The developed LTCC material sinters by melting a glassy phase at a temperature of 900 °C. It is known that the LTCC materials is mainly used of electronic application, where at least two different materials are needed for this propose (LTCC and conductive material). The low sintering temperature of the LTCC enables the co-sintering with high conductive metals like cooper, silver and gold. The development of the de-binding and sintering process will depend on the metal used for the final pieces, so it must be studied taking in consideration each application. In this context, the following pieces demonstrate the capability to successfully obtain complex LTCC pieces for further hybridization of technologies and multimaterial printing processes for electronic applications. Fig. 12 shows the DLP-SLA during the printing process of a propeller-like geometry parts and the green bodies, demonstrating the feasibility of the developed LTCC suspensions for a top-down DLP-SLA machine with a light source.

4. Conclusions

The development LTCC suspension at 40.4 vol% accomplishes the requirements for its printability by DLP-SLA, demonstrated by some green bodies printed at different layer thickness. The optimal milling time for the optimized suspension, is achieved in a range of 50–95 h with a viscosity of 2.8 Pa s at 2 s^{-1}. The photocuring behaviour are also constant in value in this period of time, with a cure depth of 100 µm for an energy dose of 140 mJ cm^{-2}. This milling time is the one with highest interest in terms of stability of the suspension in both aspects, viscosity and photocuring behaviour.

The addition of an antifoam into the formulation improves air bubble elimination, slightly increasing the viscosity and maintaining photocuring behaviour of the LTCC suspension. The optimized LTCC has a final viscosity of 3.6 Pa s at 2 s^{-1}, meaning a viscosity 90 times higher than the SPOT-LV resin without ceramic particles. On the other hand, the sensitivity decreases 95% with the addition of the ceramic particles: the sensitivity is 850 µm for the resin and 41 µm for the optimized LTCC suspension. Concerning the critical energy dose, the values are 48 mJ cm^{-2} for the resin and 15 mJ cm^{-2} for the LTCC suspension, meaning a reduction of 69% of the energy needed to initiate the polymerization process when the ceramic particles is added.

It was demonstrated the strong correlation between particle size distribution and the resultant photocuring behaviour and viscosity during the preparation of the suspension. This correlation should have a similar effect in the preparation of ceramic suspensions for DLP-SLA

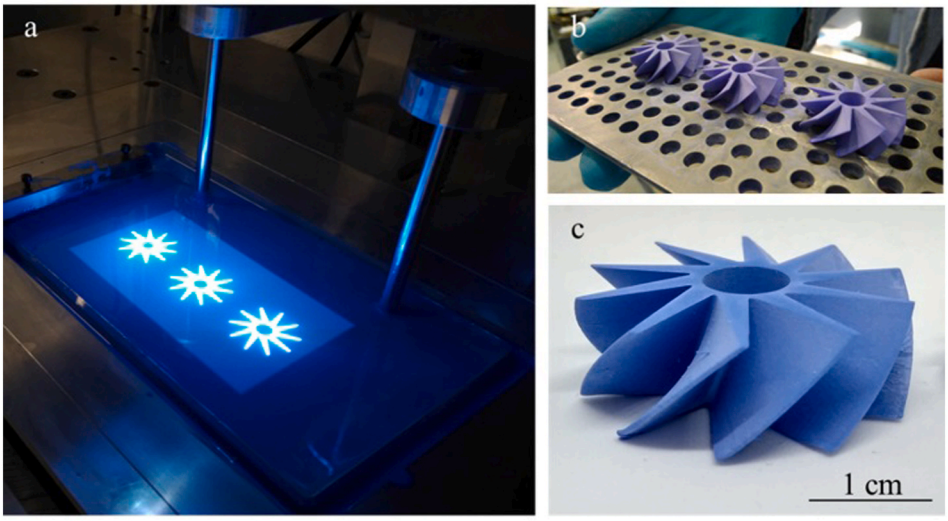

Fig. 12. Images of (a) DLP-SLA process during the printing of a propeller-like geometry, (b) green bodies in the building platform after cleaning and (c) propeller-like green body. (For interpretation of the references to colour in this figure legend, the reader is referred to the Web version of this article.)

printing.

This study highlights the importance of the standardization of the preparation of the ceramic suspension, since it directly affects both viscosity and photocuring behaviour and consequently the printing processes of ceramic suspensions for DLP-SLA.

Declaration of competing interest

The authors declare that they have no known competing financial interests or personal relationships that could have appeared to influence the work reported in this paper.

Acknowledgments

This work was supported by Spanish Government: DPI2016-80119-C3-3-R and RTC-2015-3497-7 (MINECO/FEDER), Catalan Government for *Doctorats Industrials* (DI-2014), 2017 SGR 118 and BASE 3D (001-P-001646).

References

[1] U. Scheithauer, E. Schwarzer, T. Moritz, A. Michaelis, Additive manufacturing of ceramic heat Exchanger : opportunities and limits of the lithography-based ceramic manufacturing (LCM), J. Mater. Eng. Perform. 27 (2018) 14–20, https://doi.org/10.1007/s11665-017-2843-z.

[2] Z.C. Eckel, C. Zhou, J.H. Martin, A.J. Jacobsen, W.B. Carter, T.A. Schaedler, Additive manufacturing of polymer-derived ceramics, Sci. Rep. 351 (2016) 3–8, https://doi.org/10.1126/science.aad2688.

[3] O. Santoliquido, G. Bianchi, P. Dimopoulos, Additive manufacturing of periodic ceramic substrates for automotive catalyst supports, J. Appl. Ceram. Technol. 14 (2017) 1164–1173, https://doi.org/10.1111/ijac.12745.

[4] H. Cui, R. Hensleigh, H. Chen, X. Zheng, Additive Manufacturing and size-dependent mechanical properties of three-dimensional microarchitected , high-temperature ceramic metamaterials, J. Mater. Res. 33 (2018) 360–371, https://doi.org/10.1557/jmr.2018.11.

[5] J. Brie, T. Chartier, C. Chaput, C. Delage, B. Pradeau, F. Caire, M. Boncoeur, J. Moreau, A new custom made bioceramic implant for the repair of large and complex craniofacial bone defects, J. Cranio-Maxillofacial Surg. 41 (2013) 403–407, https://doi.org/10.1016/j.jcms.2012.11.005.

[6] R. Gmeiner, G. Mitteramskogler, A.R. Boccaccini, Stereolithographic ceramic manufacturing of high strength bioactive glass, Int. J. Appl. Ceram. Technol. 45 (2015) 38–45, https://doi.org/10.1111/ijac.12325.

[7] P. Tesavibul, R. Felzmann, S. Gruber, R. Liska, I. Thompson, A.R. Boccaccini, J. Stamp, Processing of 45S5 Bioglass by lithography-based additive manufacturing, Mater. Lett. 74 (2012) 81–84, https://doi.org/10.1016/j.matlet.2012.01.019.

[8] C. Paredes, F. Vázquez, A. Pajares, P. Miranda, Development by robocasting and mechanical characterization of hybrid HA/PCL coaxial scaffolds for biomedical applications, J. Eur. Ceram. Soc. 39 (2019) 4375–4383, https://doi.org/10.1016/j.jeurceramsoc.2019.05.053.

[9] R. Galante, C. Pina, A. Serro, Additive manufacturing of ceramics for dental applications: a review, Dent. Mater. 35 (2019) 825–846, https://doi.org/10.1016/j.dental.2019.02.026.

[10] S. Hengsbach, A. Muslija, A. Muslija, X. Ren, J. Shen, R. Schittny, Lithography-based ceramic manufacture (LCM) of auxetic structures : present capabilities and challenges, Smart Mater. Struct. 25 (2016) 1–10, https://doi.org/10.1088/0964-1726/25/5/054015.

[11] M. Khosravani, T. Reinicke, 3D-printed sensors: current progress and future challenges, Sensors Actuators A Phys 305 (2020) 111916, https://doi.org/10.1016/j.sna.2020.111916.

[12] B.M. Rodríguez, PhD. Dissertation, Inkjet and Screen Printing for Electronic Applications, University of Barcelona, 2016.

[13] Y. Imanaka, Multilayered Low Temperature Cofired Ceramics, LTCC) Technology, 2005.

[14] E. MacDonald, R. Wicker, Multiprocess 3D printing for increasing component functionality, Sci. Manuf. 353 (2016) 1512–1522, https://doi.org/10.1126/science.aaf2093.

[15] J. Li, T. Wasley, T.T. Nguyen, V.D. Ta, J.D. Shephard, J. Stinger, P. Smith, E. Esenturk, C. Connaughton, R. Kay, Hybrid additive manufacturing of 3D electronic systems, J. Micromech. Microeng. 26 (2016) 1–14, https://doi.org/10.1088/0960-1317/26/10/105005.

[16] P. Sarobol, A. Cook, P.G. Clem, D. Keicher, D. Hirschfeld, A.C. Hall, N.S. Bell, Additive manufacturing of hybrid circuits, Annu. Rev. Mater. Res. 46 (2016) 41–62, https://doi.org/10.1146/annurev-matsci-070115-031632.

[17] J. Raynaud, V. Pateloup, M. Bernard, D. Gourdonnaud, D. Passerieux, D. Cros, V. Madrangeas, T. Chartier, Hybridization of additive manufacturing processes to build ceramic/metal parts: example of LTCC, J. Eur. Ceram. Soc. 40 (2020) 759–767, https://doi.org/10.1016/j.jeurceramsoc.2019.10.019.

[18] A.J. Lopes, E. Macdonald, R.B. Wicker, Integrating stereolithography and direct print technologies for 3D structural electronics fabrication, Rapid Prototyp. J. 18/2 (2012) 129–143, https://doi.org/10.1108/13552541211212113.

[19] M.T. Sebastian, H. Jantunen, Low loss dielectric materials for LTCC applications: a review, Int. Mater. Rev. (2008), https://doi.org/10.1179/174328008X277524.

[20] T. Hafkamp, G. Van Baars, B. de Jager, P. Etman, A trade-off analysis of recoating methods for vat-photopolymerization of ceramics, in: Proc. 28th Annu. Int. Solid Free, Fabr. Symp., 2017, pp. 687–711.

[21] M.L. Griffith, J.W. Halloran, Freeform fabrication of ceramics via stereolithography, J. Am. Ceram. Soc. 79 (1996) 2601–2608, https://doi.org/10.1111/j.1151-2916.1996.tb09022.x.

[22] P. Cai, G. Liang, H. Wang, J. Li, J. Li, Y. Qiu, Q. Zhang, Q. Lue, Effects of slurry mixing methods and solid loading on 3D printed silica glass parts based on DLP stereolithography', Ceram. Int. 46 (2020) 16833–16841, https://doi.org/10.1016/j.ceramint.2020.03.260.

[23] K. Zhang, C. Xie, R. He, G. Ding, M. Wang, D. Dai, D. Frang, High solid loading, low viscosity photosensitive Al2O3 slurry for stereolithography based additive manufacturing, Ceram. Int. 45 (2019) 203–208, https://doi.org/10.1016/j.ceramint.2018.09.152.

[24] Y. De Hazan, J. Heinecke, A. Weber, T. Graule, Journal of Colloid and Interface Science High solids loading ceramic colloidal dispersions in UV curable media via comb-polyelectrolyte surfactants, J. Colloid Interface Sci. 337 (2009) 66–74, https://doi.org/10.1016/j.jcis.2009.05.012.

[25] A. Goswami, K. Ankit, N. Balashanmugam, A.M. Umarji, G. Madras, Optimization of rheological properties of photopolymerizable alumina suspensions for ceramic microstereolithography, Ceram. Int. 40 (2014) 3655–3665, https://doi.org/10.1016/j.ceramint.2013.09.059.

[26] P.F. Jacobs, Fundamentals of stereolithography, 3D Syst (1992) 196–210.

[27] J. Zhang, L. Wei, X. Meng, F. Yu, N. Yang, S. Liu, Digital light processing-stereolithography three-dimensional printing of yttria-stabilized zirconia', Ceram. Int. 46 (2020) 8745–8753, https://doi.org/10.1016/j.ceramint.2019.12.113.

[28] J.W. Halloran, Ceramic stereolithography: additive manufacturing for ceramics by photopolymerization, Annu. Rev. Mater. Res. 46 (2016) 19–40, https://doi.org/10.1146/annurev-matsci-070115-031841.

[29] A. Muguruza, J. Bonada, A. Gómez, J. Minguella-Canela, J. Fernandes, F. Ramos, E. Xuriguera, A. Varea, A. Cirera, Development of a multi-material additive manufacturing process for electronic device, Procedia Manuf 13 (2017) 746–753, https://doi.org/10.1016/j.promfg.2017.09.180.

[30] G. Mitteramskogler, R. Gmeiner, R. Felzmann, S. Gruber, C. Hofstetter, J. Stampfl, J. Ebert, W. Wachter, J. Laubersheimer, Light curing strategies for lithography-based additive manufacturing of customized ceramics, Addit. Manuf. 1–4 (2014) 110–118, https://doi.org/10.1016/j.addma.2014.08.003.

[31] K. Wang, M. Qiu, C. Jiao, J. Gu, D. Xie, C. Wang, X. Tang, Z. Wei, L. Shen, Study on defect-free debinding green body of ceramic formed by DLP technology', Ceram. Int. 46 (2020) 2438–2446, https://doi.org/10.1016/j.ceramint.2019.09.237.